Turunen, Konsta; Yazdani, Maryam Roza; Santasalo-Aarnio, Annukka; Seppälä, Ari

Exceptional cold-crystallization kinetics of erythritol-polyelectrolyte enables long-term thermal energy storage

Published in:
Solar Energy Materials and Solar Cells

DOI:
10.1016/j.solmat.2021.111273

Published: 15/09/2021

Document Version
Publisher's PDF, also known as Version of record

Solar Energy Materials & Solar Cells 230 (2021) 111273

Contents lists available at ScienceDirect

Solar Energy Materials and Solar Cells

journal homepage: www.elsevier.com/locate/solmat

Exceptional cold-crystallization kinetics of erythritol-polyelectrolyte enables long-term thermal energy storage

Konsta Turunen *, Maryam Roza Yazdani, Annukka Santasalo-Aarnio, Ari Seppälä

Department of Mechanical Engineering, Aalto University School of Engineering, FI-00076 Aalto, Espoo, Finland

ARTICLE INFO

Keywords:
Thermal energy storage
Phase change material
Erythritol
Supercooling
Cold-crystallization
Crystallization kinetics

ABSTRACT

Long-term thermal energy storage balances the seasonal variations in renewable energy supply and demand, but applied storage concepts require improved performance in efficiency, reliability and capacity. In principle, supercooling and cold-crystallization offer a way to store heat for an extensive amount of time. In this approach, crystallization behaviour of the material governs the storage performance, as it directly relates to optimal efficiency, length of the storage period and heat release properties. This work explains the unique cold-crystallization behaviour of erythritol in cross-linked sodium polyacrylate. To this end, isothermal cold-crystallization was measured experimentally and analysed with the Avrami equation. Although the cold-crystallization rate constant follows the Arrhenius equation, it drastically decreases near the glass transition region and diverges from the equation. Thermal history also influences the cold-crystallization behaviour. Increases in cooling end-temperature reduce the subsequent crystallization time and promote metastable polymorph formation. These findings stem from the peculiar energy landscape of erythritol in cross-linked sodium polyacrylate. The landscape is classified as kinetically strong and thermodynamically fragile, which facilitates long-term thermal energy storage. Consistent supercooling and cold-crystallization behaviour of the material enables predicting the time-dependent crystallization rate at different temperatures. This confirms applicability of the two-stage Arrhenius-VFT model for temperature dependence and supports storage design in real-life applications.

1. Introduction

Implementation of renewable energy sources is challenged by large diurnal and seasonal variations. As a result, energy storages are exploited to obtain efficient renewable energy systems. Long-term thermal energy storage (TES) captures otherwise wasted excess energy streams from an energy abundant period, storing the energy for weeks to months. When high demand emerges, the energy is released as heat. Such sustainable technology benefits countries with large seasonal variations in energy production and demand.

The main challenges of long-term TES are related to the heat losses and storing the enormous volumes of collected energy [1,2]. Typically, long-term TES technologies are installed underground and operate by the means of sensible heat, for instance, heating and cooling water as a storage medium. Storage volume can be reduced by applying phase change materials (PCMs) with high energy densities. PCMs store and release large amounts of heat during phases change of melting and solidification. PCMs large-scale use is still limited as they suffer from drawbacks, such as shorter durability compared sensible TES and low thermal conductivity impeding the charging and discharging of the strorage [3–5]. In addition to PCMs, thermochemical storages have shown great potential in long-term TES, as they offer minimal heat losses and the largest energy density among the three described methods. However, thermochemical TES is still at a laboratory scale and must overcome hurdles in material development and system design, such high cost and poor heat and mass transfer [6,7].

Supercooling of a PCM can be exploited to minimize heat losses during the storage stage [8]. This phenomenon occurs when a PCM remains in a liquid phase below the equilibrium melting temperature (T_m). If crystallization is avoided in the supercooled state, the latent heat of melting can be stored for as long as needed. In fact, supercooling TES has been applied in heating pads, where sodium acetate trihydrate (SAT) stores the latent heat of melting while supercooling [9]. SAT shows a large melting heat and an appropriate melting temperature for domestic TES applications [10]. Similarly, polyols, such as erythritol and xylitol, possess suitable melting properties for TES applications and experience

* Corresponding author.
E-mail address: konsta.turunen@aalto.fi (K. Turunen).

https://doi.org/10.1016/j.solmat.2021.111273
Received 15 February 2021; Received in revised form 26 May 2021; Accepted 29 June 2021
Available online 9 July 2021

large supercooling degrees [11].

However, the drawback of the supercooled TES materials is that the metastability of the supercooled state hinders the reliability and applicability of the storage. Factors, such as rough edges, pressure differences, incongruent melting and mechanical stress can initiate spontaneous crystallization, releasing the stored heat prematurely [8,12]. The probability of nucleation also increases by the volume of the material. This has been evidenced for SAT, as laboratory scale TES systems regularly released the latent prematurely [13,14], yet research on overcoming the metastability of SAT continues [14]. Polyols suffer from the same drawback as well. On the other hand, materials such as xylitol, can show stable supercooling, but suffer from low crystallization rates that result in inadequate heat release rates [15]. Absence of a simple and a reliable initiation method for the heat release can also complicate the large-scale usage of the supercooled TES [16].

Exploiting glass transition and cold-crystallization solves the impediments of the supercooled TES materials. If the supercooled material is further cooled without crystallization, it will vitrify and form an amorphous solid (or glass) below the glass transition temperature (T_g). In the glassy state, molecules are unable to relax to a crystal structure within experimental times. In fact, already in the deeply supercooled state (T_g<T < 1.2T_g (K)) crystallization time can increase significantly and enable reliable long-term TES [17]. During re-heating of such system, molecules can overcome the energy barrier of relaxation to a crystal structure and induce crystallization. Herein, this process of crystallization caused by re-heating from glassy or supercooled state is referred as cold-crystallization. The principle of supercooling and cold-crystallizing TES has been demonstrated in a milligram scale by using metal-complexes [18], structurally confined polyols [19,20], and polyol-polymer mixtures [21,22].

Typically, PCMs spontaneously crystallize during supercooling, but sugar alcohols, such as erythritol and xylitol, can experience large degrees of supercooling and even vitrify upon further cooling [11,23,24]. Additives, such as polymers and cross-linking agents, can adjust supercooling, vitrification and cold-crystallization properties of the active storage material. For example, erythritol within ionically cross-linked polyvinyl alcohol exhibited stable supercooling, shape-stability and high melting and cold-crystallization heat up to 266 J/g and 157 J/g, respectively [22]. Moreover, 160 g samples of erythritol in cross-linked sodium polyacrylate demonstrated exceptional TES capability by storing the melting heat without reduction for at least three months in the supercooled state (0 °C–10 °C) [17]. At higher storage temperatures, the material slowly crystallized, gradually releasing the stored heat from a day to month time scale.

As evidenced by the challenges and the operational principle, crystallization (nucleation and crystal growth) governs the functionality of supercooled TES. Particularly for the cold-crystallizing materials, storage temperatures above the glass transition induce slow cold-crystallization, and influence the optimal storage temperature and time. Whereas, cold-crystallization at higher temperatures directly correlates to the heat release rate. This necessitates the investigation of cold-crystallization characteristics which can improve the design and predict the operation of a supercooled TES system. Characterization of the supercooling and the cold-crystallization behaviour is not straightforward. Vitrification can be regarded as an interplay between the characteristic time for crystallization and structural relaxation. The temperature dependence of the crystallization time results from the competition between growth kinetics and thermodynamic driving force for nucleation, causing the crystallization time to first decrease, then to increase with the degree of supercooling [25]. On the other hand, the structural relaxation time demonstrates a steep increase with the extent of supercooling, eventually becoming so large that crystallization cannot occur within the experimental time frame, meaning that the material has vitrified. The relaxation time correlates to the viscosity of the material, which can deviate between the glass-forming materials. For example, according to the strong-fragile classification [26], the viscosity of kinetically strong liquids, such as SiO_2, display Arrhenius-type temperature dependence in a wide temperature range. Whereas, fragile liquids, such as glycerol, deviate significantly from the Arrhenius behaviour [27]. One way to analyse the conversion degree from melt to solid phase is by applying the Avrami equation [28,29]: $\alpha = 1 - exp(-Kt^n)$. This equation describes the phase change kinetics in stretched exponential function form, which can be applied in diverse kinetic investigations. It is particularly used to analyse polymer crystallization, as it can yield useful information about mechanisms of the macromolecule crystallization; especially for the simple cases, such as spherulite crystallization with constant crystal growth rate [30].

Herein, we explain exceptional TES capability of erythritol in cross-linked sodium polyacrylate matrix (CCM) by analysing its cold-crystallization behaviour. To this end, the structure of CCM was examined using optical microscope, SEM and XRD, and thermal durability was measured with TGA. The crystallization kinetics was explored by measuring isothermal cold-crystallization in the supercooled region from 1.1T_g to 1.3T_g (K) with a differential scanning calorimetry (DSC). The DSC data was modelled with the Avrami equation, exhibiting an excellent fit. Successful Avrami analysis resulted in the crystallization rate constants (k_c) at varying temperatures, which showed Arrhenius-type temperature dependence and a drastic divergence from the relationship, when glass transition region was approached. Furthermore, measurements revealed that the thermal history prior cold-crystallization significantly influences the crystallization rate and the formation of the metastable polymorph of CCM.

2. Materials and methods

2.1. Material preparation

CCM consisted of erythritol in a cross-linked sodium polyacrylate network, which is prepared following the method described by Puupponen and Seppälä [21]. The polymer network was prepared in aqueous erythritol (technical grade, supplied by Suomen Luontaistukku Ltd. Finland) by polymerizing acrylic acid (assay ≥99%, supplied by Merck). Acrylic acid was first neutralized with sodium hydroxide (assay ≥99%, supplied by VWR Chemicals), then polymerization was initiated by adding 0.1 wt% potassium persulfate (assay ≥98%, supplied by VWR Chemicals). The molar neutralization degree was 100%. Cross-linking of sodium polyacrylate was accomplished using 2 wt% of ethylene dimethacrylate (assay ≥97.5%, supplied by Merck).

The properties and crystallization behaviour of CCM can be adjusted by altering the composition. In order to evaluate the impact of the composition on the crystallization behaviour, three compositions were prepared with varied mass fractions of erythritol: CCM-75, CCM-80 and CCM-85 containing 75 wt%, 80 wt% and 85 wt% of erythritol. The amount of sodium polyacrylate was 22.9 wt%, 17.9 wt% and 12.9 wt%, respectively.

2.2. Characterization methods

Cold-crystallization rate of CCM was measured under isothermal conditions using differential scanning calorimetry (Netzsch DSC204F1 Phoenix DSC). Since the crystallization rate strongly depends on temperature, CCM samples were crystallized in the temperature range from 0 °C to 65 °C with 5 °C intervals, corresponding the range from 1.1T_g to 1.3T_g (K). DSC Program 1 consisted of four steps. First, the measurement sample was melted at 135 °C, followed by cooling to −60 °C at 5 K/min. Then, the heating step of 20 K/min increased the sample temperature to the isothermal cold-crystallization temperature. Lastly, isothermal step from one to 15 h maintained the temperature of the sample at a constant level until the cold-crystallization was fully completed. For each isothermal crystallization temperature, the described program was completed at least two twice. The influence of the erythritol-polymer ratio was revealed using three CCM samples with different

compositions. The sample masses were 25.00 ± 0.06 mg.

As the cold-crystallization rate abruptly reduced in the deeply supercooled state (T_g<T < 1.2T_g (K)), conventional DSC measurement loses accuracy. Therefore, Program 2 estimated the crystallization rate for CCM-80 in the deeply supercooled state at 0 °C, 5 °C and 10 °C by using DSC and a thermal chamber. Program 2 followed DSC Program 1 until the isothermal cold-crystallization temperature was reached, after which the sample was quickly removed from DSC and placed in a thermal chamber. Temperature of the chamber was maintained at 0 ± 0.1 °C, 5 ± 0.1 °C and 10 ± 0.1 °C. After a specified crystallization period (t_{iso}) from 6 h to 12 days, the sample was quickly placed inside DSC to measure cold-crystallization heat (ΔH_{cc}) and temperature (T_{cc}) during a heating step of 0.5 K/min. Undergoing Program 2 yielded the progress of crystallization only at the time $t = t_{iso}$. In comparison, Program 1 estimated the progress of crystallization for the entire crystallization process. Therefore, Program 2 was repeated at least five times with different crystallization period at each temperature. To determine thermophysical properties of CCM, melting heat (ΔH_m) and temperature (T_m) and cold-crystallization heat and temperature were measured in DSC using 0.5 K/min heating and cooling steps between −60 °C and 135 °C without a storage period. The glass transition temperature (T_g) was determined from the transition mid-point during 0.5 K/min, 5 K/min, 10 K/min and 20 K/min heating rate.

Further characterization of CCM was conducted with CCM-80, as it represents the average of the tested compositions. The amorphous to crystalline structure was analysed using Rigaku SmartLab X-ray diffractometer, where Linkam heating-cooling stage (HFSX-350-GI) controlled the temperature of the sample under a nitrogen atmosphere. The XRD measurement began by melting the sample at 150 °C, and then cooling it to −120 °C, to reach glassy state. Next, the temperature was increased stepwise (−30 °C, 35 °C, 45 °C and 65 °C), to observe cold-crystallization.

The morphology of CCM-80 was investigated using scanning electron microscope (JEOL JSM-7500FA) with 1.5 kV acceleration voltage. A powder sample was prepared by melting the sample at 130 °C, cooling it to −20 °C and then cold-crystallizing at 50 °C. Lastly, the sample was ground in a mortar. Furthermore, polarized optical microscope (Leica DM4500) imaged isothermal cold-crystallization of CCM-80. During cold-crystallization, constant temperature was maintained with Linkam heating stage. In addition, thermogravimetric analyser (TA TGA Q500) estimated the decomposition temperature in the range from room temperature to 900 °C with 10 K/min heating, to determine the operational temperature range of CCM-80.

3. Results and discussion

3.1. Crystal morphology

Isothermal cold-crystallization process of CCM-80 was imaged using polarized microscope at 50 °C. The sample was first melted at 130 °C, and cooled to −20 °C. Thereafter, it was re-heated and maintained isothermally at 50 °C until cold-crystallization was completed. Fig. 1 shows images of the crystallization process. At the beginning, crystals grew freely, forming spherical crystals (Fig. 1A). As the crystallization progressed, spherical growth were limited by other crystals (Fig. 1C), eventually filling the entire imaged area (Fig. 1D). In the early stage of crystallization (Fig. 1A), crystals displayed a faint dark Maltese cross, which is characteristic for a spherulite under polarized light [31]. Similarly, spherulitic crystals have been observed in pure erythritol, when it is crystallized at high supercooling degrees [32] and during re-heating from the glassy state [23]. These findings confirm the spherical crystal growth of CCM under the tested environment. However, the crystals are not perfectly spherical, especially at the later stages of crystallization, as depicted in Fig. 1B.

Furthermore, the surface morphology of CCM-80 and erythritol was imaged with scanning electron microscope, shown in Fig. 2. While bulk erythritol displays smooth surface in SEM images (Fig. 2A), CCM-80's images reveal fibrillar-type surface structure of the crystal (Fig. 2B). These crystal structures originate from the center of the crystal growing in radial direction, as observed in optical microscope images (Fig. 1).

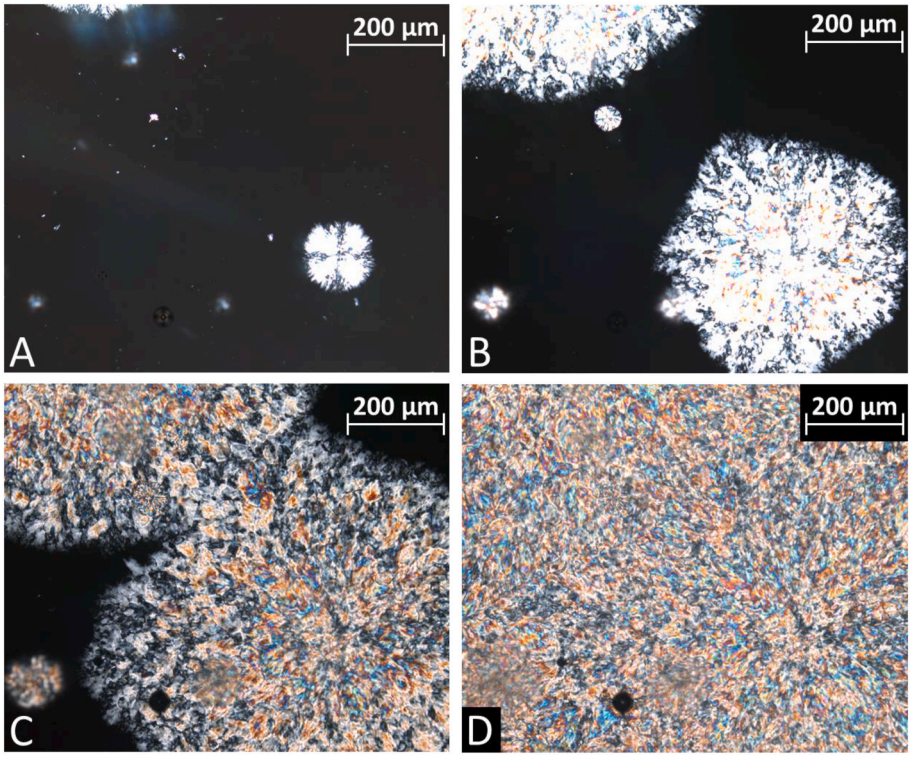

Fig. 1. Polarized optical microscope images of CCM-80's spherical cold-crystallization, when the sample was melted at 130 °C, cooled to −20 °C and cold-crystallized at 50 °C. The images from A to D were recorded at 5 min intervals.

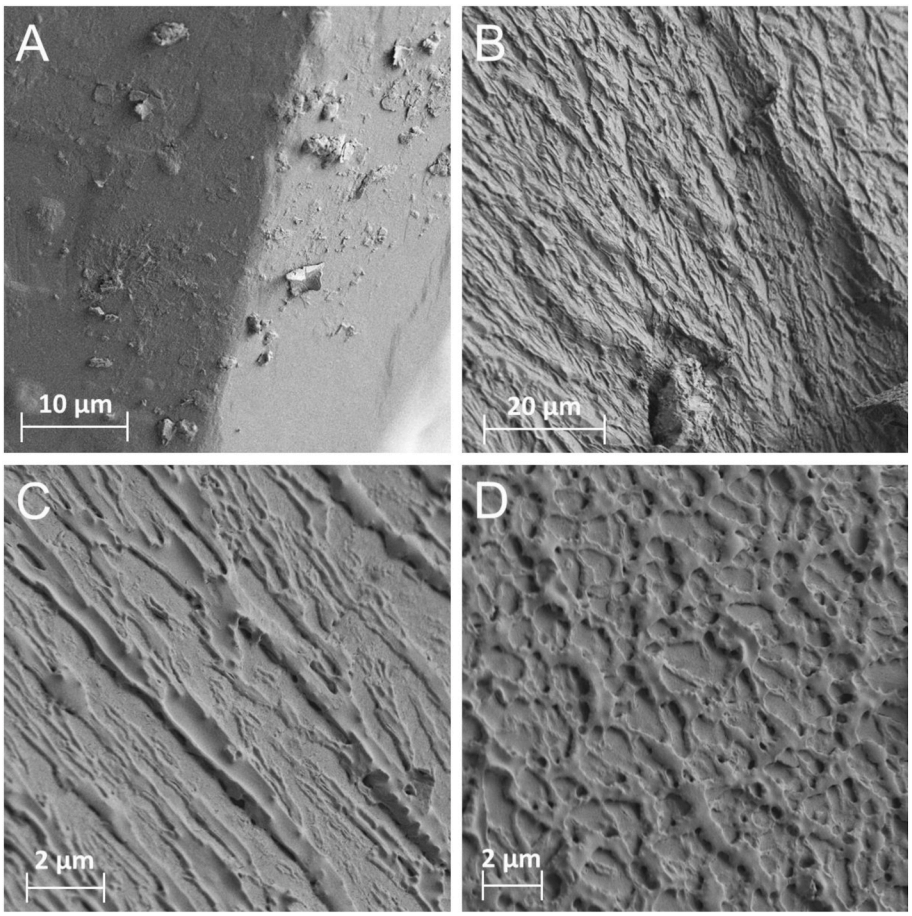

Fig. 2. Scanning electron microscope images of pure erythritol (A) and CCM-80 (B–D). Images A and B depict the difference in the surface morphology of erythritol and CCM, while C and D illustrate CCM's surface from a different orientation of the crystal growth.

Similar type of spherulitic growth has been observed under SEM imaging when polyethylene glycol mixed with polyurethane cold-crystallized [33]. In addition to fibrillar structure, SEM images also revealed network-type structural pattern (Fig. 2D). The difference in Fig. 2C and D can be explained by the orientation of the imaged CCM particles, which yielded images perpendicular and parallel to the direction of crystal growth. These crystallization patterns of CCM-80 indicate a homogenous spread of the erythritol in the polymeric matrix. The homogenous polymer structure inhibits the mobility of the crystallizing erythritol, causing the fibrillar-type crystal morphology and imperfect spherical growth. Indeed, spherical crystallization of polymers and polymer blends can be limited by the self-diffusion of the crystallizing material, as its molecular movement is restricted by the interactions of the stagnant material's molecules [34].

3.2. Isothermal cold-crystallization

As differential scanning calorimetry (DSC) measures heat flow, the effect of nucleation and crystal growth cannot be separately observed. Nevertheless, their simultaneous effect on crystallization can be described by the Avrami equation [28,29], which can be presented as in Eq. (1) and Eq. (2).

$$\alpha = 1 - exp(-Kt^n) \tag{1}$$

$$\log[-\ln(1-\alpha(t))] = n \log t + \log K \tag{2}$$

$$\alpha(t) = \frac{X_c(t)\rho_l}{\rho_c - X_c(t)(\rho_c - \rho_l)} \tag{3}$$

Here, t is the time from the beginning of the crystallization (s), K a parameter dependent on the nucleation rate and the growth rate and n a parameter describing the type of nucleation and the dimensionality of the crystallization process, also referred to as Avrami index. The conversion degree from liquid to crystal phase, $\alpha(t)$, is defined as the volume fraction of the crystal phase. It is calculated by Eq. (3), where ρ is density (kg/m^3) and $X_c(t)$ is the mass fraction of crystal phase measured by DSC. Subscript l refers to the liquid and c to the crystal phase.

Eq. (2) can be fitted to the conversion degree data to form an Avrami plot, in which $\log[-\ln(1-\alpha(t))]$ is against $\log t$. This enables graphical determination of the parameters K and n from the interception and the slope of the fitted line. Fig. 3 illustrates the Avrami plot for selected temperatures of the tested compositions. In Fig. 3C, slow cold-crystallization of CCM-80 was measured at low temperatures using DSC program 2.

The Avrami equation has received criticism due to its simple formulation, as parameters K and n might change as the crystallization process progresses [31,35]. Nonetheless, the Avrami equation has shown validity in computer simulation and experimental work, and it can reveal useful information of the crystallization process, especially for simple nucleation and crystal growth cases [30,31]. Our previous work showed that CCM-80 corresponds to Avrami equation in a wide conversion degree range from 0.05 to 0.80 [36]. In this work, we use the same conversion degree range for the analysis and expand the analysed compositions and temperature range.

As indicated by Fig. 3, crystallization behaviour of CCM samples corresponds to Eq. (2). The coefficient of determination (R^2) for the fitted Eq. (2) varies mainly around 0.9990 ranging from 0.9954 to 0.99998 for all the measurements with DSC Program 1. In contrast, R^2

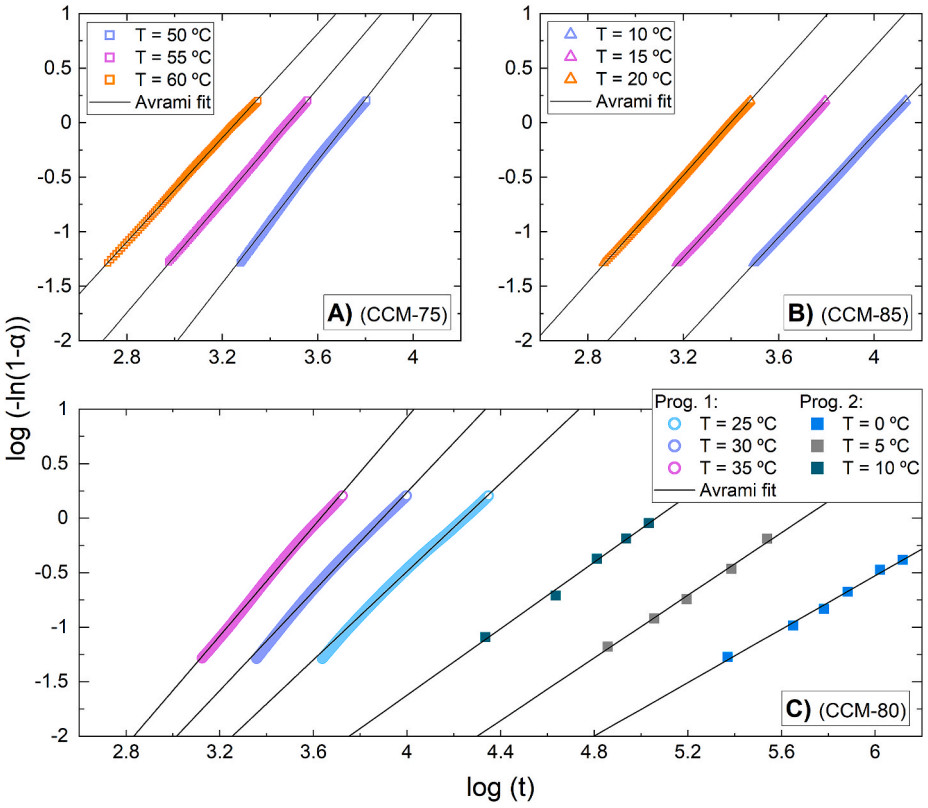

Fig. 3. Avrami plots for CCM-75 (A), CCM-85 (B) and CCM-80 (C). CCM-80 was measured also at 0 °C, 5 °C and 10 °C using Program 2.

value of 0.9990 or larger is proposed to indicate very good fit in the Avrami plot [30]. Therefore, all CCM compositions show consistent crystallization behaviour in the large conversion degree range from 0.05 to 0.80. Fig. 3C shows the Avrami plot for CCM-80, when crystallization occurred also in the deeply supercooled state (0 °C, 5 °C and 10 °C). The linear trend of the data points indicates that crystallization mechanism does not change during crystallization, similar to measurements at higher temperatures. The data from DSC Program 2 shows larger deviations from the fitted lines, compared to continuous DSC measurements (DSC Program 1) as evidenced by the R^2 values of 0.993, 0.995 and 0.995 for 0 °C, 5 °C and 10 °C, respectively. This could be caused by the different measurement method, where factors such as stochastic nature of crystallization and uniform chamber temperature deviate the results.

Since the parameter n (Avrami index) is dependent on the mechanisms of nucleation and crystal growth, it can reveal helpful information on the nature of the crystallization. In DSC Program 1 measurements, values of n scatter around 2.5 (Fig. S1) with average values of 2.49 ± 0.19, 2.17 ± 0.15 and 2.42 ± 0.10 for CCM-75, CCM-80 and CCM-85, respectively. Theoretically, Avrami equation yields $n = 2.5$ for the case of constant nucleation rate and three-dimensional spherical crystal growth with growth rate depending on the square root of time (diffusion-controlled growth). This appears reasonable, as DSC samples are three-dimensional and spherical crystal were observed with optical microscope (Fig. 1). Similarly, equivalent value could be achieved by other crystallization cases, for example by axialitic crystallization aided by heterogenous nucleation [30]. CCM-80 appears to yield lower values than CCM-75 and CCM-85 which can be caused by number of factors. First, the stochastic nature of crystallization causes some deviations in the crystallization of CCM-80, such as imperfect spherical growth displayed under optical microscope (Fig. 1). Secondly, impurities and preferred nucleation sites can also induce secondary nucleation reducing Avrami index in the range from 0 to 1 [37]. CCM-80's high number of thermal cycles may also influence the crystallization behaviour. Nonetheless, Avrami index is consistent with the tested CCMs and corresponds to the value around 2.5 reported previously for CCM with similar composition [36].

Crystallization of CCM-80 was also analysed in the deeply supercooled state (T_g<T < 1.2T_g (K)) at 0 °C, 5 °C and 10 °C. These temperatures yielded Avrami index of around 1.23, 1.43 and 1.52, which are illustrated as smaller slopes of the Avrami fit in Fig. 3C. The decreasing trend of Avrami index indicates an increasing dominance of nucleation compared to crystal growth. This is supported by bulk scale measurements, as CCM forms numerous millimetre-scale crystals at 0 °C and fewer larger crystals at 5 °C [17]. The reduction in Avrami index appears to behave linearly and begin at the cross-over to deeply supercooled region at below 1.2T_g (25 °C for CCM-80). Intriguingly, below this temperature CCM-80 shows further changes in crystallization behaviour, which are discussed in the following sections.

3.3. Temperature dependence of cold-crystallization

In order to analyse the temperature dependence of the crystallization rate, parameter K is transformed to crystallization rate constant: $k_c = K^{1/n}$ (s^{-1}). The dependence can be then described applying Arrhenius equation:

$$k_c = k_0 * \exp\left(\frac{-E_a}{RT}\right) \quad (4)$$

where R is the universal gas constant (J/K·mol) and E_a (J/mol) and k_0 (1/s) are fitting parameters. Here, the parameter E_a expresses the activation energy for cold-crystallization. When $\ln(k_c)$ is plotted against 1/T, the fitting parameters can be defined from the slope $-E_a/R$ and interception at $\ln\ (k_0)$.

Fig. 4 depicts the temperature dependence of the crystallization rate constant of CCM samples when the temperature is scaled by T_g. The k_c shows linear temperature dependence following Arrhenius equation, for

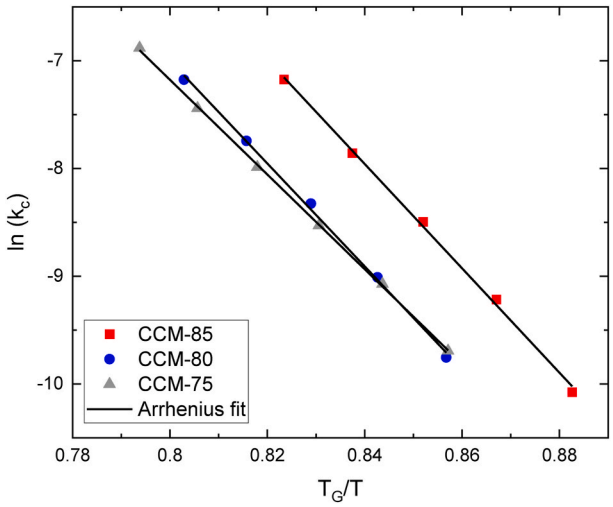

Fig. 4. Comparison of the temperature dependence of the crystallization rate constant (k_c) for the tested CCM samples.

which fitting parameters are listed in Table 1. Tested compositions behave similarly, as their values of E_a result around 100 kJ/mol. This corresponds with the observations made in the Avrami equation analysis (Fig. 3). As erythritol content of CCM decreases, the crystallization rate at constant temperature significantly reduces. This is expected as compositions with less erythritol contain larger amount of polymer, leading to increased molecular interactions between the erythritol and the polymer, and manifesting as higher glass transition temperature (T_g) and stability. The T_g scaling in Fig. 4 also shows that CCM-80 and CCM-75 have overlapping values, while CCM-85 deviates from the two. Therefore, it appears that the crystallization rate of CCM could be characterized using T_g in the erythritol fraction range from 75 wt% to 80 wt%.

The different behaviour of CCM-85 could be caused by a significant increase of erythritol's molecular mobility in the composition with a small polymer-to-erythritol ratio. Erythritol within sodium polyacrylate matrix can exist in free, freezing-bound or non-freezing bound states. Free erythritol, if exists, melts and crystallizes as pure erythritol, while freezing-bound erythritol is under moderate influence of the polymer and is still capable of phase transition. In contrast, non-freezing-bound erythritol is strongly influenced by the polymer and is incapable of phase transition. Because CCM did not show phase transition at the melting temperature of pure erythritol (T_m~119 °C), freezing-bound erythritol melts and crystallizes in CCM. The mass fraction of freezing-bound erythritol can be calculated as $B_f = \Delta H_{m,CCM}/(W_{ERY} * \Delta H_{m,ERY})$. Consequently, CCM-85 yields B_f ~0.83, which is higher value compared to CCM-80 (0.64) and CCM-75 (0.53). This increment implies an increased mobility, as less erythritol is strongly influenced by the polymer matrix.

Table 1
Thermophysical properties and fitting parameters of Arrhenius equation. T_g is defined from the mid-point of glass transition during 5 K/min heating step, while other thermophysical properties during 0.5 K/min heating step. Values of E_a include standard error.

	Thermophysical properties						Arrhenius parameters	
	T_m [K]	ΔH_m [J/g]	T_{cc} [K]	ΔH_{cc} [J/g]	T_g [K]	m	E_a [kJ/mol]	$\ln(k_0)$
CCM-75	379	162	330	113	261	16.1	98.1 ± 0.9	28.0
CCM-80	380	183	311	130	249	15.8	101.4 ± 2.5	31.2
CCM-85	384	245	290	135	240	15.6	98.9 ± 2.3	32.7

Thermophysical properties of CCM are also listed in Table 1. Melting heat is a key parameter of CCM, as it describes the long-term TES capacity. It ranges from 162 J/g to 245 J/g, which yield energy densities of approximately 230 MJ/m^3 and 350 MJ/m^3, when density of CCM-80 (1430 kg/m^3) is used [17]. For comparison, the same energy density is achieved by increasing water temperature by 55 °C and 85 °C, respectively. This places CCM in the mid-range of low and medium temperature phase change materials, which typically range from 100 to 500 MJ/m^3 [4]. In principle, entire melting heat could be discharged, if crystallization occurred at the melting temperature. However, as cold-crystallization begins in a supercooled state, dischargeable heat obeys equation $\Delta H_{cc} = \Delta H_m - \int_{T_{cc}}^{T_m} (C_{p,l} - C_{p,s}) dT$, where $C_{p,l}$ and $C_{p,s}$ are the specific heat capacities for liquid and solid state, respectively. Consequently, dischargeable heat reduces as the cold-crystallization temperature decreases. The reduction in the latent heat can be illustrated by the ratio of cold-crystallization and melting heat, $\Delta H_{cc}/\Delta H_m$, i.e. the efficiency of the latent heat storage. It ranges from 0.55 to 0.71 for CCM in the DSC environment of this work. This efficiency could be increased, if CCM is cold-crystallized at higher temperature, for example, by faster heating during initiation of cold-crystallization. Storage efficiency among other storage performance indicators of CCM are analysed in detail in our previous work [17].

3.4. Kinetic fragility

When temperature of the supercooled liquid decreases, the viscosity increases abruptly, especially when approaching the glass transition region. This viscous slowdown can be characterized by the concept of liquid fragility. Viscosity of kinetically strong liquids follow Arrhenius-type temperature dependence and kinetically fragile liquids deviate from the Arrhenius behaviour [27,38]. The deviation can be quantified by the kinetic fragility parameter, m, which is defined in Eq. (5) and Eq. (6) [38].

$$m = \left(\frac{d \log x}{d\left(\frac{T_g}{T}\right)} \right)_{T=T_g} = \frac{E_g}{T_g \ln 10} \tag{5}$$

$$\frac{E_g}{R} = \frac{d \log q}{d \log\left(1/T_g\right)} \tag{6}$$

where x is a dynamic variable, such as viscosity or relaxation time and E_g activation energy at glass transition temperature. Fragility values typically range from 16 to 200, where small values indicate strong and large values fragile behaviour [38,39]. CCM yields m ~16, categorizing it as kinetically strong liquid. This is consistent with similar CCM compositions and polyvinyl alcohol-erythritol mixtures, which have demonstrated small kinetic fragility values in the range from 14 to 20 [21,22]. Determination of E_g is illustrated in Fig. S2.

Fig. 5 shows the crystallization rate constant of CCM-80 in the tested temperature range. Arrhenius equation accurately estimates k_c until 0.00353 1/K (10 °C), but drastically overestimates the values above it, that is below 10 °C. Therefore, the transition to non-Arrhenius behaviour occurs at around 10 °C, which equals 1.14T_g for CCM-80. Divergence of the kinetic properties from the Arrhenius relation is well-known in the realm of glass-forming liquids. This behaviour is typically described applying the Vogel-Fulcher-Tammann (VFT) equation [27]. The VFT equation can be formulated for the crystallization rate constant as Eq (7).

$$k_c = k_r * \exp\left(\frac{B}{T - T_r}\right) \tag{7}$$

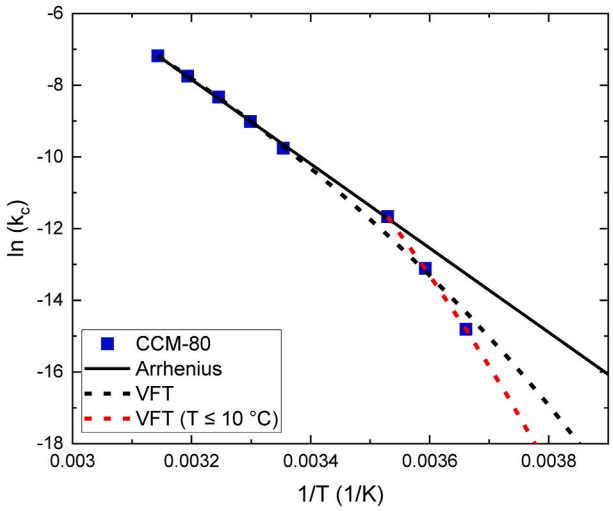

Fig. 5. Crystallization rate constants of CCM-80 with Arrhenius and VFT fittings. VFT (T ≤ 10 °C) refers to a curve which was fitted to the data at 0.00353 1/K and above.

$$m = \frac{\frac{B}{T_g}}{\ln 10\left(1 - \frac{T_r}{T_g}\right)^2} \tag{8}$$

where k_r, B and T_r are fitting parameters. In this study, crystallization rate constant is the relevant dynamic variable in the VFT equation, which also resembles Arrhenius equation. If T_r equals zero, the equation yields the Arrhenius equation. Furthermore, VFT equation relates to kinetic fragility through the kinetic fragility parameter, as formulated in Eq. (8) [38,39]. VFT equation has successfully described the non-Arrhenius behaviour of numerous glass-forming liquids for decades. For example, VFT equation accurately predicts the viscosity behaviour of sorbitol and glycerol, even at temperatures close to T_g [40,41]. However, the equation has shown to breakdown for some materials when approached to glass transition temperature [25,42].

As shown in Fig. 5, VFT equation shows better correspondence to k_c compared to the Arrhenius equation. However, it fails to accurately fit the crystallization data at low temperatures, as k_c is underestimated at 0.00353 1/K (10 °C) and overestimated at 0.00366 1/K (0 °C). The best fit of VFT equation yields fitting parameter values described in Table 2. Consequently, fragility parameter based on VFT fitting results in $m = 45$, which is larger than the one calculated by Eq. (5) ($m = 16$). Therefore, the crystallization rate cannot be accurately modelled using Arrhenius or VFT equation unless the temperature range is divided in sections. When the analysed range is limited to T ≤ 10 °C, VFT shows correspondence to k_c with the fitting parameters listed in Table 2. In this case, m equals 71, which is similar to the fragilities of hydrogen bonded organics with T_g in the same temperature range as CCM-80 [39]. In fact, hydrogen bonding liquids show peculiar behaviour, for example alcohols display intermediate kinetic fragility, but large thermodynamic fragility. Thermodynamic fragility can be defined as the ratio of liquid and glassy state specific heat capacity at T_g ($C_{p,l}/C_{p,g}$) [26,27]. Typically, strong glass formers yield small ratio of $C_{p,l}/C_{p,g}$~1.1, whereas fragile liquids have larger values. Similarly, CCM-80 has large thermodynamic fragility of $C_{p,l}/C_{p,g}$~1.8, categorizing it as thermodynamically fragile liquid. Therefore, CCM-80 demonstrates kinetically strong and thermodynamically fragile behaviour. This means that CCM-80 displays a unique energy landscape, which consists of many low-energy configurations, such as a fragile liquid, but the barriers between the minima are high, such as a strong liquid [26]. Erythritol's conformational flexibility and strong ion-dipole forces between the polymer and the erythritol generate this unique energy landscape. It provides conditions for stable supercooling and slow crystallization rates in the deeply supercooled state (T_g<T < 1.2T_g (K)), enabling long-term storing of the latent heat.

To contextualize these results, a material system samples its entire energy landscape at sufficiently high temperatures, during which majority of the sampled energy minima are shallow. Therefore, the activation energy for structural relaxation displays temperature independent behaviour. However, as the system is cooled to deeply supercooled region, kinetic energy decreases and dynamics become influenced by the energy landscape. Consequently, the activation energy begins to increase during cooling. Furthermore, decoupling of translational diffusion and viscosity, and rotational and translational diffusion occurs below around 1.2T_g [43]. These changes in dynamics explain qualitatively the steep change in the crystallization rate constant from Arrhenius type to VFT type temperature dependence at 1.14T_g. In addition, change in crystallization mechanism was observed in Section 3.2, as the Avrami index begins to decrease at around 1.2T_g (~25 °C for CCM-80) indicating increasing dominance of nucleation over crystal growth. It appears that CCM's kinetically strong and thermodynamically fragile behaviour facilitates this type of change in the temperature dependence of the crystallization. Therefore, viscosity and diffusion ought to exhibit changes in their temperature dependence at around 1.14T_g, as well. Crystallization is influenced by several factors from material's dynamic properties to mechanism of nucleation and crystal growth. For example, the crystal growth rate has shown decoupling from viscosity close to glass transition region, and this decoupling appeared to increase with the fragility of the material, in a way that strong liquids remained coupled [44]. Crystal growth time of glycerol (m ~50) has also indicated decoupling from self-diffusion coefficient near T_g [45]. These types of decouplings, depending on the extent, ought to influence CCM's cold-crystallization. Further investigation on the kinetics at the deeply supercooled state, for example by measuring the viscosity of CCM, ought to reveal more of the interplay between the dynamic properties and crystallization behaviour.

The behaviour of the rate constant, k_c, indicates that it can be modelled using two-stages in a way that Arrhenius equation (Table 1) estimates k_c above 10 °C and VFT equation (Table 2) below 10 °C. In order to verify the applicability of this two-stage model, we used it to calculate the conversion degree and the heat flow of CCM-80's isothermal cold-crystallization, and compared the calculations to the measured data. The conversion degree was calculated with Eq. (1), where k_c is estimated using the two-stage model and the Avrami index, n, is obtained from Avrami analysis in Section 3.2. Below 10 °C linear interpolation was used to determine n (see Section 3.2). Fig. 6 plots conversion degree model and data and the heat flow during CCM-80's isothermal cold-crystallization. Sample was cooled to −60 °C before cold-crystallization. The calculated curves for 0 °C, 5 °C and 10 °C, shown in Fig. 6A, coincide with the data resulting in R^2 values above 0.994. In addition, a predicted curve at 7 °C corresponds to a DSC measurement at the same temperature, confirming accurate results predicted by VFT model and linear interpolation of Avrami index. As DSC measures heat flow, we ought to compare the modelled and the measured heat flow curves during isothermal cold-crystallization. Differentiation of Eq. (1) yields the heat flow over time for isothermal cold-crystallization, which is exemplified in Fig. 6B. The heat flow curves were calculated using Avrami indices defined in Section 3.2 and k_c values from Arrhenius equation (Table 1). As a result, the modelled heat flow curves correspond to the measurement data with R^2 values ranging

Table 2
Fitting parameters of VFT equation for the tested temperature range and below 10 °C (3.53 10^{-3} … 3.66 10^{-3} 1/K).

Temperature range [1/K]	ln(k_r)	B[K]	T_r[K]
3.14 10^{-3} … 3.66 10^{-3}	8.21	2180	176
3.53 10^{-3} … 3.66 10^{-3}	15.50	2680	185

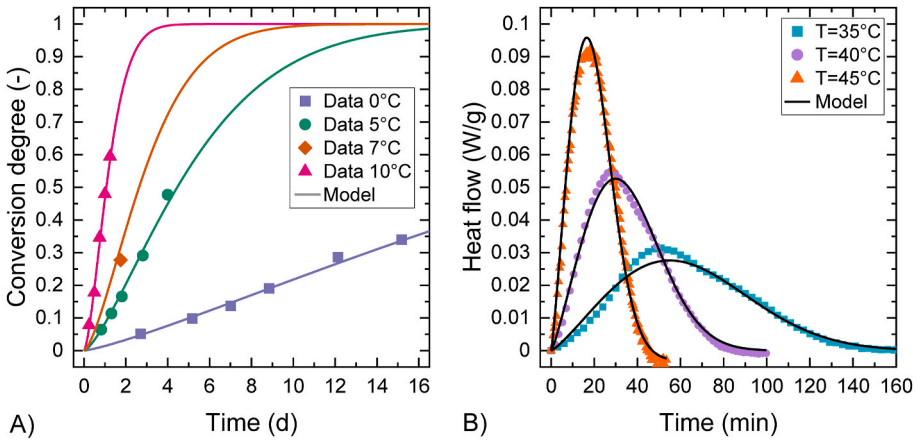

Fig. 6. (A) Conversion degree of CCM-80 at constant cold-crystallization temperatures. Curves were determined using Eq. (1), where k_c was obtained from VFT equation and n by linear interpolation. Data at 0 °C, 5 °C and 10 °C was used for modelling, while 7 °C data for verifying model. (B) Heat flow during isothermal cold-crystallization of CCM-80 measured by DSC (symbol) and fits calculated from Eq. (1) (line). The values of k_c were estimated by Arrhenius equation and the values of n were determined in Avrami analysis in Section 3.2. Sample was cooled to −60 °C before cold-crystallization in both figures.

from 0.960 to 0.997. In Fig. 6B, R^2 values are 0.981, 0.992 and 0.997 for 35 °C, 40 °C and 45 °C, respectively. Some deviations between the modelled and the measured curves ought to occur because of the stochastic nature of crystallization. Nonetheless, the two-stage model coincides with the conversion degree and the heat flow data of cold-crystallization, verifying the applicability of the two-stage model and Avrami equation for describing the isothermal crystallization rate of CCM-80. In the future, the two-stage model and Avrami equation can be used to predict the crystallization rate at the storage temperature and in the beginning of the heat release. Predictability of CCM's cold-crystallization rate is essential for applications, as it enables determining suitable storage temperature and time, as well as the maximum heat release rates in the beginning of the storage discharge. Conversion degree and heat flow shown in Fig. 6 depict the accuracy of the modelling in reasonable experimental time scale. In a TES application, appropriate thermal history and storage temperature would be used to enable efficient storage for several months. An analysis on the time evolution of CCM's dischargeable heat with a suitable temperature history for long-term TES can be found in a previously conducted investigation [17].

3.5. Polymorphism

Erythritol has two known polymorphs, the stable form is polymorph I (T_m~119 °C), and metastable is polymorph II (T_m~105 °C). In principle, both polymorphs can form when erythritol is crystallized from a deeply supercooled state [23]. Nevertheless, CCM indicated formation of the stable polymorph I, exhibiting a single melting peak and consistent IR band in accordance to bulk erythritol [21]. Fig. 7 depicts the XRD spectra of bulk erythritol and CCM-80 at room temperature and during cold-crystallization. Comparison of CCM-80 and bulk erythritol under XRD (Fig. 7A) and FTIR (Fig. S3) confirm that CCM-80 crystallized into stable polymorph I at room temperature, as the corresponding peaks coincide. CCM-80 displayed lower peak intensities in Fig. 7A, especially at 2θ = 14.5, 19.5 and 20.1°, which are the characteristic peaks of erythritol [46]. The decreased peak intensities are caused by the existence of non-freezing bound erythritol, which does not melt or crystallize. As explained in Section 3.3, the freezing-bound erythritol has a value of 0.64, which contributes to the peak intensities.

Fig. 7B depicts the XRD spectra of CCM-80 at several temperatures, when the sample was liquid at 150, °C cooled to −120 °C and heated in a stepwise manner. CCM-80 showed no signs of crystal phase after the cooling to glassy sate, confirming a stable supercooling. During the subsequent heating, a crystal phase began to form at 35 °C, and at higher scanning temperatures crystallization was completed. Emerged peaks correspond to that of bulk erythritol (Fig. 7A), confirming crystallization to polymorph I.

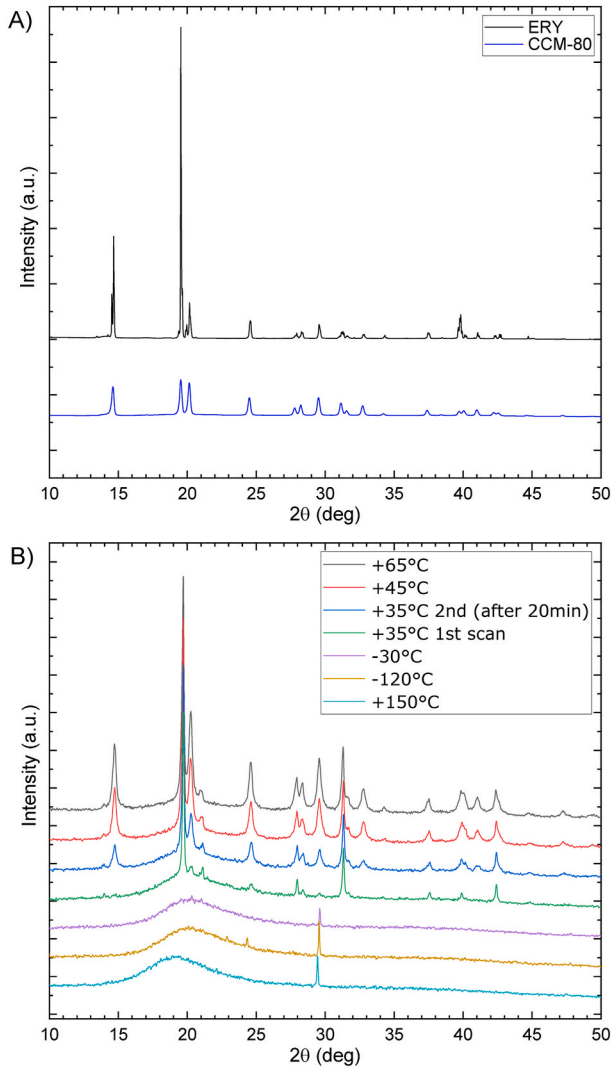

Fig. 7. (A) X-ray diffraction spectra of CCM-80 and erythritol at room temperature. (B) Crystallization profile of CCM-80 under in-situ temperature X-ray diffraction measurement. The sample was melted at 150 °C, then cooled to −120 °C. Consequent heating was conducted stepwise for scanning the sample. The peak at 2θ = 29.5° (scans at 150 °C, −120 °C and −30 °C) corresponds to silicon wafer underneath the sample, as the sample was in a melted or a glassy state. (For interpretation of the references to colour in this figure legend, the reader is referred to the Web version of this article.)

However, DSC measurements with CCM-80 indicated that polymorph II can form under certain circumstances. Among the cooling end-temperatures in DSC measurements (−60 °C, −28 °C, −10 °C, −5 °C and 0 °C), polymorph II emerged only when cooled to 0 °C. Fig. 8 illustrates the occurrence and DSC thermographs of the polymorphs when the cooling end-temperature was 0 °C. The polymorph formations in Fig. 8A imply that T_{cc} below 50 °C favours polymorph I, while polymorph II becomes increasingly frequent at 50 °C and higher. These results indicate that the probability of forming metastable polymorph II increases under higher cooling end-temperatures and higher cold-crystallization temperatures. On the other hand, CCM did not crystallize at all in some of the cycles when it was cooled to 0 °C. At lower cooling temperatures, CCM crystallized every time. Therefore, increasing the cooling end-temperature appears to also inhibit crystal formation after subsequent heating. Nevertheless, the bulk scale of 160 g CCM showed tendency to crystallize every time, when re-heated from 0 °C [17].

The DSC thermograph of the melting process depicted in Fig. 8B yielded a melting heat and temperature of 177 J/g and 107 °C for polymorph I, and 141 J/g and 92 °C for polymorph II. These melting temperatures of CCM showed the same temperature difference between the polymorphs as erythritol, confirming that CCM can crystallize to the two known erythritol polymorphs. Reduced melting temperatures of the two polymorphs for CCM is caused by the presence of non-freezing-bound erythritol in the system (see Section 3.3).

As illustrated in Fig. 9, The crystallization rate of polymorph II is slower than polymorph I. For example, at 50 °C polymorph II crystallizes in approximately 4 h, while polymorph I in approximately 1 h, when the cooling end-temperature was 0 °C. By comparing the crystallization rate of polymorph I and polymorph II, the specific polymorphs formation could be deduced during DSC measurements. As the crystallization rates matched the corresponding melting temperatures of polymorph I and II, no solid-solid transformation occurred in DSC measurements. In the work of Lopes Jesus et al. [23], pure erythritol showed transformation from polymorph II to polymorph I between the crystallization and melting temperature of polymorph II. The unique behaviour of CCM, can be explained by the strong intermolecular interactions between the polymer and erythritol. These interactions slow down the molecular movement, causing prolonged transformation durations. Time period in DSC measurements were not sufficient for the solid-solid transformation. However, given longer time periods, the transformation ought to occur.

Erythritol molecules experience conformational flexibility, causing numerous possible molecular conformations [47]. For example, *meso*--erythritol has shown to adopt two conformations in the crystal structure [48], as well as indicated existence of a third conformation in an experimental work [23]. This can affect the cold-crystallization of CCM in two ways. First, the crystallization tendency can decrease, as the suitable molecular conformation must be sampled for the certain crystal structure to occur. Molecules must also reorient themselves to the crystallizing conformation, impeding the crystallization process [49]. Consequently, polymorph II crystallizes slower and requires higher energy level than polymorph I to form, because the conformations of the stable polymorph I are more likely to exist than those of polymorph II. Secondly, it is probable that polymorphs I and II are a consequence of the existence of numerous possible molecular conformations. Therefore, increasing the cold-crystallization and cooling end-temperature would increase the probability of sampling suitable conformations for polymorph II.

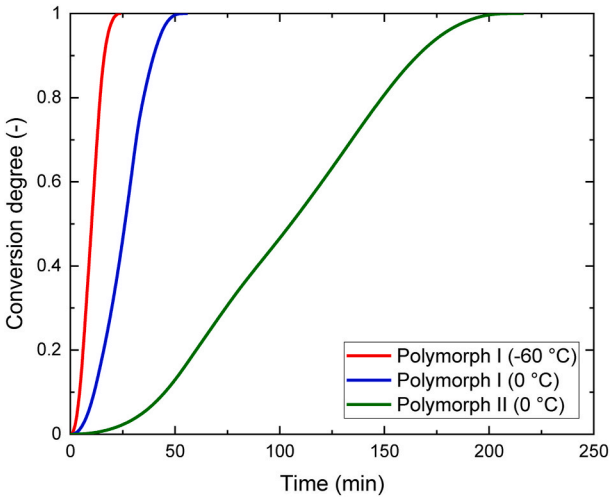

Fig. 9. The effect of polymorphism and cooling end-temperature on the isothermal crystallization time of CCM-80 at 50 °C. Cooling end-temperature are indicated in parentheses.

Polymorphism increases operational unreliability of CCM by altering the heat release and melting behaviour. Nonetheless, results indicate that crystallization to polymorph II is a rare event that requires the lowest cooling temperature of 0 °C or higher for the studied composition. In conclusion, crystallization temperature of approximately 50 °C is needed for repetitive formation of polymorph II in DSC measurements. Scaling up the sample size from milligram to gram scale might also influence the occurrence of polymorph II, as no indication of the formation of polymorph II was been observed in previous studies of CCM [17,21]. Therefore, the impact of polymorph II appears to be minimal in the bulk scale operation, yet should not be ruled out.

3.6. Thermal history

The effect of thermal history on isothermal cold-crystallization of CCM-80 was investigated by calculating crystallization rate constant (k_c) based on Avrami analysis (Section 3.2.), and cooling the sample to −60 °C, −28 °C, −10 °C, −5 °C and 0 °C before cold-crystallization. These temperatures relate to glass transition region, since CCM-80 is in the glassy state at −60 °C, middle of vitrification at −28 °C, beginning of vitrification at −10 °C and supercooled at −5 °C and 0 °C, as illustrated in Fig. S4.

As shown in Fig. 10, thermal history tests revealed that the crystallization rate constant is dependent on the cooling end-temperature. As polymorph II was infrequent and its crystallization rate was slow (see Fig. 9), we analysed the cold-crystallization rate of the dominant polymorph I in detail. As evidenced by Fig. 10, k_c decreases at a given crystallization temperature when the cooling end-temperature increases. This type of reduction in the crystallization rate appears unintuitive, because crystallization takes place at the same temperature (T_{cc}), where for example viscosity should be constant. Nonetheless, this phenomenon could relate to the conformational flexibility of erythritol, as

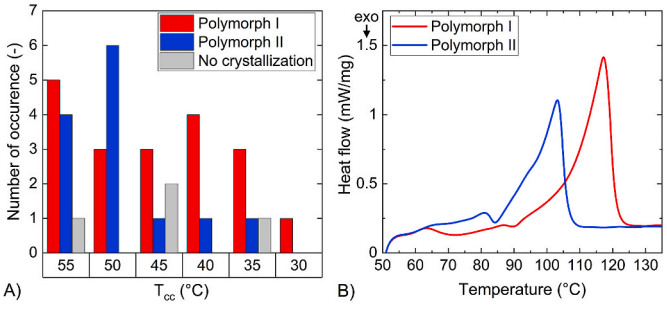

Fig. 8. (A) Occurrence of the stable polymorph I, the metastable polymorph II and no crystallization at different crystallization temperatures. Sample was cooled to 0 °C prior crystallization. (B) DSC thermograph of CCM-80's melting peaks when it was crystallized to metastable polymorph I (blue) and stable polymorph II (red). (For interpretation of the references to colour in this figure legend, the reader is referred to the Web version of this article.)

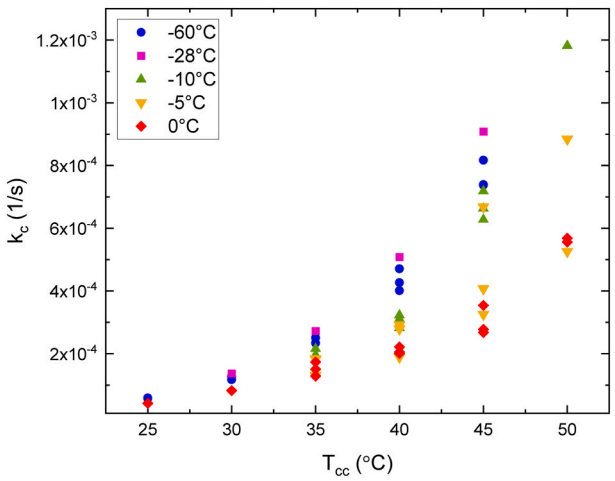

Fig. 10. The impact of cooling end-temperature on the cold-crystallization rate constant (k_c) of CCM-80 at constant cold-crystallization temperatures (T_{cc}).

discussed in Section 3.5. When material vitrifies, molecules begin to display short-range periodicity, which is characteristic for a glassy system. As the system becomes more arrested, molecules might prefer the conformations for crystal polymorph I in CCM, or the conformations that are similar. As the cooling end-temperature is increased, more thermal energy is available for sampling more conformations. Therefore, lower cooling temperatures expedite cold-crystallization, since more preferred crystal conformations exist at the initial stage. This would explain the slowdown of CCM's crystallization rate, when cooling was ended at −10 °C–0 °C. The slowdown is evidenced in Fig. 10, where the values of k_c with cooling end-temperature above −10 °C begin to show significant reductions compared to the values of k_c with cooling to −28 °C and −60 °C. Vitrification of CCM-80 begins at around −10 °C (Fig. S4).

We demonstrated the impact of the cooling end-temperature to the cold-crystallization rate also in bulk scale of 100 g, which is shown in the time-lapse video provided in the supplementary information. Fig. 11 summarizes bulk scale cold-crystallization process, where cooling to low temperatures as −20 °C has a significant incremental effect on the subsequent cold-crystallization rate at the room temperature (~20 °C). The crystallization times at the room temperature were approximately 8 h, 1 d, 3 d and 10 d for the cooling end-temperatures of −20 °C, 0 °C, 10 °C and 20 °C, respectively. An accurate estimation of the crystallization time based on the images is challenging, yet they demonstrate the impact of the cooling end-temperature evidently. Lower cooling end-temperature also reduces the size and increases the number of the crystals, implying increasing dominance of the nucleation over the crystal growth. Crystallization temperature of 20 °C was used to demonstrate CCM's crystallization behaviour in an appropriate experimental time scale. In a TES application, long-term storage would be conducted at lower temperatures, for example 0–10 °C, to prevent heat loss because of crystallization [17]. Nonetheless, the impact of the cooling end-temperature should be considered in the TES applications, and could act as an adjustable parameter to optimize the storage conditions and heat release of CCM. For example, CCM could be first cooled to a low temperature, then heated to the storage temperature. Thus, the stored heat can be released faster and at lower temperatures compared to directly cooling CCM to the storage temperature. Whereas, the disadvantage of this method is the need for additional cooling and a reduction of the efficient storage time, as crystallization occurs faster also at the storage temperature.

In addition, thermogravimetric analysis (TGA) was conducted for CCM-80, to determine the durability of the material. Fig. S5 illustrates the TGA analysis for CCM-80 and erythritol. Decomposition of CCM-80 begins at around 150 °C, and plateaus when 80% of the mass is lost. This corresponds to the mass fraction of erythritol. At approximately 450 °C, mass loss increases, as sodium polyacrylate decomposes. Therefore, CCM-80's maximum operational temperature limits to around 150 °C, which is in the same range as erythritol. This confirms the stability of CCM under the operational temperature range that was up to 130 °C. As erythritol is the main component in CCM, these results indicate that other CCM composition have similar operational temperature range.

4. Conclusions

This work discovers the phenomena behind the unique long-term TES capability of erythritol in cross-linked sodium polyacrylate (CCM) and demonstrates predictability of the material's cold-crystallization

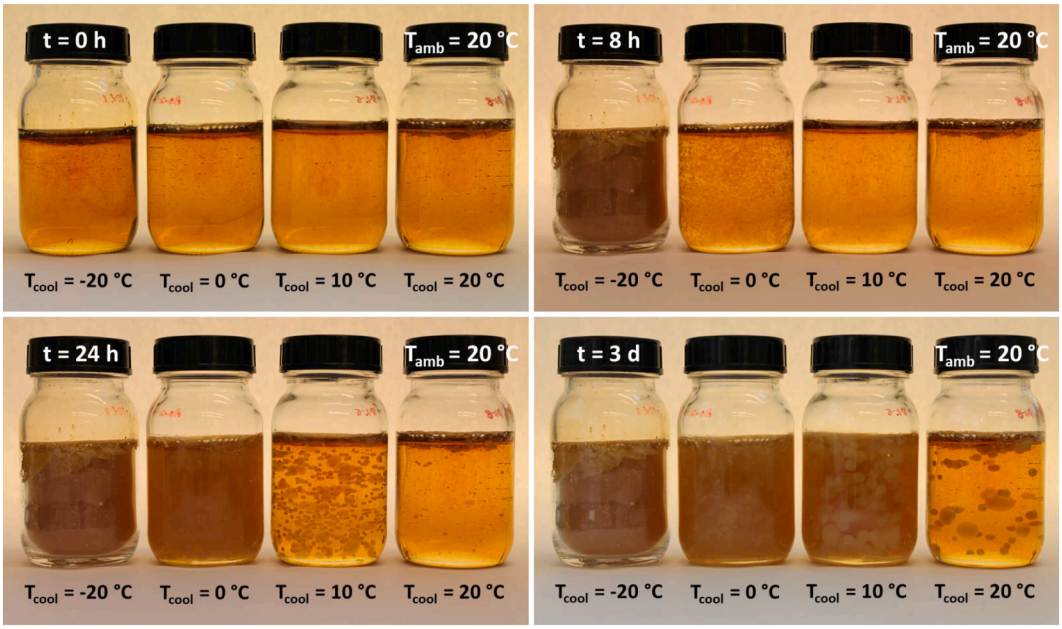

Fig. 11. Cold-crystallization of bulk CCM-80 samples (100 g) at the room temperature (T_{amb} ~20 °C). Prior crystallization, samples were melted at 130 °C, and cooled and stored at T_{cool} = −20 °C, 0 °C, 10 °C or 20 °C for 12 h.

behaviour. Three CCM compositions with erythritol mass fractions of 75 wt%, 80 wt% and 85 wt% were investigated, because erythritol-to-polymer fraction changes the cold-crystallization and TES properties. Optical microscopy revealed spherical cold-crystallization of CCM. Furthermore, cold-crystallization of all CCM compositions followed the Avrami equation in the tested temperature range from $1.1T_g$ to $1.3T_g$ (K), which enables modelling and prediction of CCM's cold-crystallization rate.

We found that the temperature dependence of the crystallization rate constant follows Arrhenius equation from $1.14T_g$ to $1.3T_g$. Below $1.14T_g$, the rate constant drastically decreases, diverging from the equation. The VFT equation also failed to accurately model the entire temperature range, yet it fit the data below $1.14T_g$, indicating that a two-stage model can predict the crystallization rate of CCM. In the future, the two-stage Arrhenius-VFT model could be used to estimate heat release rates and efficient storage periods at different temperatures, which are crucial parameters for a reliable CCM based TES. The drastic reduction of the rate constant is one of the key characteristics of CCM, as it enables effective long-term TES at a practical temperature level of 0 °C and higher. Practical storage temperature level is essential for efficient TES operation, because external cooling can be minimized during the storage period. From a physical perspective, behaviour of the rate constant can be qualitatively understood by the transition to energy-landscape influenced behaviour below $1.2T_g$. CCM's strong ion-dipole forces between the polymer and erythritol constitute a peculiar energy-landscape which can be categorized as kinetically strong and thermodynamically fragile. This explains CCM's exceptional supercooling stability and cold-crystallization behaviour for efficient storing of heat for several months.

Thermal history below $1.2T_g$ also influenced the crystallization characteristics of CCM. Erythritol's metastable polymorph II formed during isothermal cold-crystallization that was preceded by cooling to 0 °C. In contrast, polymorph II was not observed in any other of the cooling end-temperatures in DSC (from −60 °C to 0 °C), XRD and FTIR. Moreover, isothermal cold-crystallization time of the stable polymorph I doubled, when cooling end-temperature was increased from −60 °C to 0 °C. This is a significant finding in terms of CCM based TES operation, since the cooling end-temperature, that is typically the storage temperature, influences the cold-crystallization rate during the following heat release stage. The cooling end-temperature acts as an adjustable parameter for operation of CCM based TES. For example, increased heat release rates are achieved by decreasing the cooling end-temperature prior the storage stage. The findings in this work reveal physical nature of using cold-crystallization for predictable long-term TES, forwarding efficient exploitation of renewable energy sources.

CRediT authorship contribution statement

Konsta Turunen: Conceptualization, Methodology, Software, Validation, Formal analysis, Investigation, Writing – original draft, Visualization, Project administration, Funding acquisition. **Maryam Roza Yazdani:** Conceptualization, Methodology, Investigation, Writing – review & editing, Visualization. **Annukka Santasalo-Aarnio:** Conceptualization, Writing – review & editing, Supervision, Visualization. **Ari Seppälä:** Conceptualization, Resources, Writing – review & editing, Supervision, Funding acquisition.

Declaration of competing interest

The authors declare that they have no known competing financial interests or personal relationships that could have appeared to influence the work reported in this paper.

Acknowledgements

This work is extended version of the research presented in the 14th International Renewable Energy Storage Conference 2020 (IRES 2020). This work was supported by the Maj and Tor Nessling Foundation (201900332), Business Finland (HeatStock project), and Technology Industries of Finland Centennial Foundation and Jane and Aatos Erkko Foundation (Future Makers 2019 Program). The research made use of OtaNano Nanomicroscopy Center (NMC). The authors wish to acknowledge D.Sc. Salla Puupponen for her valuable comments.

Appendix A. Supplementary data

Supplementary data to this article can be found online at https://doi.org/10.1016/j.solmat.2021.111273.

References

[1] G. Alva, Y. Lin, G. Fang, An overview of thermal energy storage systems, Energy 144 (2018) 341–378, https://doi.org/10.1016/j.energy.2017.12.037.
[2] T. Kousksou, P. Bruel, A. Jamil, T. El Rhafiki, Y. Zeraouli, Energy storage: applications and challenges, Sol. Energy Mater. Sol. Cells 120 (2014) 59–80, https://doi.org/10.1016/j.solmat.2013.08.015.
[3] S. Wu, T. Yan, Z. Kuai, W. Pan, Thermal conductivity enhancement on phase change materials for thermal energy storage: a review, Energy Storage Mater 25 (2020) 251–295, https://doi.org/10.1016/j.ensm.2019.10.010.
[4] H. Nazir, M. Batool, F.J.B. Osorio, M. Isaza-ruiz, X. Xu, K. Vignarooban, P. Phelan, Inamuddin, A.M. Kannan, Recent developments in phase change materials for energy storage applications: a review, Int. J. Heat Mass Tran. 129 (2019) 491–523, https://doi.org/10.1016/j.ijheatmasstransfer.2018.09.126.
[5] K. Kant, A. Shukla, A. Sharma, Advancement in phase change materials for thermal energy storage applications, Sol. Energy Mater. Sol. Cells 172 (2017) 82–92, https://doi.org/10.1016/j.solmat.2017.07.023.
[6] Y. Zhang, R. Wang, Sorption thermal energy storage: concept, process, applications and perspectives, Energy Storage Mater 27 (2020) 352–369, https://doi.org/10.1016/j.ensm.2020.02.024.
[7] A. Mehari, Z.Y. Xu, R.Z. Wang, Thermal energy storage using absorption cycle and system: a comprehensive review, Energy Convers. Manag. 206 (2020) 112482, https://doi.org/10.1016/j.enconman.2020.112482.
[8] A. Safari, R. Saidur, F.A. Sulaiman, Y. Xu, J. Dong, A review on supercooling of phase change materials in thermal energy storage systems, Renew. Sustain. Energy Rev. 70 (2017) 905–919, https://doi.org/10.1016/j.rser.2016.11.272.
[9] B. Sandnes, The physics and the chemistry of the heat pad, Am. J. Phys. 76 (2008) 546–550, https://doi.org/10.1119/1.2830533.
[10] M. Kenisarin, K. Mahkamov, Salt hydrates as latent heat storage materials: thermophysical properties and costs, Sol. Energy Mater. Sol. Cells 145 (2016) 255–286, https://doi.org/10.1016/j.solmat.2015.10.029.
[11] S.N. Gunasekara, R. Pan, J.N. Chiu, V. Martin, Polyols as phase change materials for surplus thermal energy storage, Appl. Energy 162 (2016) 1439–1452, https://doi.org/10.1016/j.apenergy.2015.03.064.
[12] M. Hasan Zahir, S.A. Mohamed, R. Saidur, F.A. Al-sulaiman, Supercooling of phase-change materials and the techniques used to mitigate the phenomenon, Appl. Energy 240 (2019) 793–817, https://doi.org/10.1016/j.apenergy.2019.02.045.
[13] M. Keinänen, in: Latent Heat Recovery from Supercooled Sodium Acetate Trihydrate Using a Brush Heat Exchanger, Helsinki Univeristy of Technology, 2007. http://urn.fi/URN:NBN:fi:aalto-2020120553783.
[14] G. Wang, M. Dannemand, C. Xu, G. Englmair, S. Furbo, J. Fan, Thermal characteristics of a long-term heat storage unit with sodium acetate trihydrate, Appl. Therm. Eng. 187 (2021) 116563, https://doi.org/10.1016/j.applthermaleng.2021.116563.
[15] A. Seppälä, A. Meriläinen, L. Wikström, P. Kauranen, The effect of additives on the speed of the crystallization front of xylitol with various degrees of supercooling, Exp. Therm. Fluid Sci. 34 (2010) 523–527, https://doi.org/10.1016/j.expthermflusci.2009.11.005.
[16] M. Dannemand, J.M. Schultz, J.B. Johansen, S. Furbo, Long term thermal energy storage with stable supercooled sodium acetate trihydrate, Appl. Therm. Eng. 91 (2015) 671–678, https://doi.org/10.1016/j.applthermaleng.2015.08.055.
[17] K. Turunen, M.R. Yazdani, S. Puupponen, A. Santasalo-Aarnio, A. Seppälä, Cold-crystallizing erythritol-polyelectrolyte: scaling up reliable long-term heat storage material, Appl. Energy 266 (2020) 114890, https://doi.org/10.1016/j.apenergy.2020.114890.
[18] K. Iwase, Y. Nagano, I. Yoshikawa, H. Houjou, Y. Yamamura, K. Saito, Cold crystallization in schiff-base nickel(II) complexes derived from three toluidine isomers, J. Phys. Chem. C 118 (2014) 27664–27671, https://doi.org/10.1021/jp5081516.
[19] K. Nakano, Y. Masuda, H. Daiguji, Crystallization and melting behavior of erythritol in and around two-dimensional hexagonal mesoporous silica, J. Phys. Chem. C 119 (2015) 4769–4777, https://doi.org/10.1021/jp510048g.
[20] S. Puupponen, V. Mikkola, T. Ala-Nissila, A. Seppälä, Novel microstructured polyol–polystyrene composites for seasonal heat storage, Appl. Energy 172 (2016) 96–106, https://doi.org/10.1016/J.APENERGY.2016.03.023.
[21] S. Puupponen, A. Seppälä, Cold-crystallization of polyelectrolyte absorbed polyol for long-term thermal energy storage, Sol. Energy Mater. Sol. Cells 180 (2018) 59–66, https://doi.org/10.1016/j.solmat.2018.02.013.

[22] M.R. Yazdani, J. Etula, J.B. Zimmerman, A. Seppälä, Ionic cross-linked polyvinyl alcohol tunes vitrification and cold-crystallization of sugar alcohol for long-term thermal energy storage, Green Chem. 22 (2020) 5447–5462, https://doi.org/10.1039/d0gc01427c.
[23] A.J. Lopes Jesus, S.C.C. Nunes, M.R. Silva, A.M. Beja, J.S. Redinha, Erythritol: crystal growth from the melt, Int. J. Pharm. 388 (2010) 129–135, https://doi.org/10.1016/j.ijpharm.2009.12.043.
[24] E. Palomo del Barrio, A. Godin, M. Duquesne, J. Daranlot, J. Jolly, W. Alshaer, T. Kouadio, A. Sommier, Characterization of different sugar alcohols as phase change materials for thermal energy storage applications, Sol. Energy Mater. Sol. Cells 159 (2017) 560–569, https://doi.org/10.1016/j.solmat.2016.10.009.
[25] P.G. Debenedetti, Metastable Liquids - Concepts and Principles, Princeton University Press, New Jersey, USA, 1996.
[26] C.A. Angell, Relaxation in liquids, polymers and plastic crystals - strong/fragile patterns and problems, J. Non-Cryst. Solids 131–133 (1991) 13–31, https://doi.org/10.1016/0022-3093(91)90266-9.
[27] C.A. Angell, Formation of glasses from liquids and biopolymers, Science 80 (267) (1995), https://doi.org/10.1126/science.267.5206.1924, 1924–1935.
[28] M. Avrami, Kinetics of phase change. I general theory, J. Chem. Phys. 7 (1939) 1103–1112, https://doi.org/10.1063/1.1750380.
[29] M. Avrami, Kinetics of phase change. II transformation-time relations for random distribution of nuclei, J. Chem. Phys. 8 (1940) 212–224, https://doi.org/10.1063/1.1750631.
[30] A.T. Lorenzo, M.L. Arnal, J. Albuerne, A.J. Müller, DSC isothermal polymer crystallization kinetics measurements and the use of the Avrami equation to fit the data: guidelines to avoid common problems, Polym. Test. 26 (2007) 222–231, https://doi.org/10.1016/j.polymertesting.2006.10.005.
[31] E. Piorkowska, G.C. Rutledge, in: Handbook of Polymer Crystallization, first ed., John Wiley & Sons, Incorporated, 2013.
[32] M. Duquesne, A. Godin, E. Palomo del Barrio, F. Achchaq, Crystal growth kinetics of sugar alcohols as phase change materials for thermal energy storage, Energy Procedia 139 (2017) 315–321, https://doi.org/10.1016/j.egypro.2017.11.214.
[33] K. Pielichowska, M. Nowak, P. Szatkowski, B. Macherzynska, The influence of chain extender on properties of polyurethane-based phase change materials modified with graphene, Appl. Energy 162 (2016) 1024–1033, https://doi.org/10.1016/j.apenergy.2015.10.174.
[34] L.M. Di Lorenzo, Spherulite growth rates in binary polymer blends, Prog. Polym. Sci. 28 (2003) 663–689, https://doi.org/10.1016/S0079-6700(02)00035-7.
[35] E. Piorkowska, A. Galeski, J. Haudin, Critical assessment of overall crystallization kinetics theories and predictions, Prog. Polym. Sci. 31 (2006) 549–575, https://doi.org/10.1016/j.progpolymsci.2006.05.001.
[36] K. Turunen, A. Santasalo-Aarnio, A. Seppälä, Storage efficiency of cold-crystallizing long-term heat storage material, in: 14th Int. Renew. Energy Storage Conf. 2020 (IRES 2020), Atlantis Press, 2021, pp. 186–192, https://doi.org/10.2991/ahe.k.210202.027.
[37] L.A. Pérez-Maqueda, J.M. Criado, J. Málek, Combined kinetic analysis for crystallization kinetics of non-crystalline solids, J. Non-Cryst. Solids 320 (2003) 84–91, https://doi.org/10.1016/S0022-3093(03)00023-1.
[38] R. Böhmer, K.L. Ngai, C.A. Angell, D. Plazek, Nonexponential Relaxations in strong and fragile glass formers, J. Chem. Phys. 99 (1993) 4201–4209, https://doi.org/10.1063/1.466117.
[39] Q. Qin, G.B. Mckenna, Correlation between dynamic fragility and glass transition temperature for different classes of glass forming liquids, J. Non-Cryst. Solids 352 (2006) 2977–2985, https://doi.org/10.1016/j.jnoncrysol.2006.04.014.
[40] C.A. Angell, D.L. Smith, Test of the entropy basis of the vogel-tammann-fulcher equation. Dielectric relaxation of polyalcohols near Tg, J. Phys. Chem. 86 (1982) 3845–3852, https://doi.org/10.1021/j100216a028.
[41] C.A. Angell, R.C. Stall, W. Slchlna, Viscosity-temperature function for sorbitol from combined viscosity and differential scanning calorimetry studies, J. Phys. Chem. 86 (1982) 1540–1542, https://doi.org/10.1021/j100206a015.
[42] J.C. Mauro, Y. Yue, A.J. Ellison, P.K. Gupta, D.C. Allan, Viscosity of glass-forming liquids, Proc. Natl. Acad. Sci. United States Am. 106 (2009) 19780–19784, https://doi.org/10.1073/pnas.0911705106.
[43] P.G. Debenedetti, F.H. Stillinger, Supercooled liquids and the glass transition, Nature 410 (2001) 259–267, https://doi.org/10.1038/35065704.
[44] M.D. Ediger, P. Harrowell, L. Yu, Crystal growth kinetics exhibit a fragility-dependent decoupling from viscosity, J. Chem. Phys. 128 (2008), 034709, https://doi.org/10.1063/1.2815325.
[45] A. Sanz, K. Niss, Coupling between molecular mobility and kinetics of crystal growth in a hydrogen-bonded liquid, Cryst. Growth Des. 17 (2017) 4628–4636, https://doi.org/10.1021/acs.cgd.7b00484.
[46] ICDD, PDF-4+/Organics 00-033-1665, USA, 2020.
[47] A.J. Lopes Jesus, L.I.N. Tome, M.T.S. Rosado, M.L.P. Leitao, J.S. Redinha, Conformational study of erythritol and threitol in the gas state by density functional theory calculations, Carbohydr. Res. 340 (2005) 283–291, https://doi.org/10.1016/j.carres.2004.11.018.
[48] A.J. Lopes Jesus, J.S. Redinha, On the structure of erythritol and L-threitol in the solid state: an infrared spectroscopic study, J. Mol. Struct. 938 (2009) 156–164, https://doi.org/10.1016/j.molstruc.2009.09.018.
[49] L. Yu, S.M. Reutzel-Edens, C.A. Mitchell, Crystallization and polymorphism of conformationally flexible molecules: problems, patterns, and strategies, Org. Process Res. Dev. 4 (2000) 396–402, https://doi.org/10.1021/op000028v.